Quantum Electronics **45** (1) 15–22 (2015) ©2015 Kvantovaya Elektronika and Turpion Ltd

PACS numbers: 42.55.Px; 73.21.La; 85.35.Be
DOI: 10.1070/QE2015v045n01ABEH015264

Effect of parameter variations on the static and dynamic behaviour of a self-assembled quantum-dot laser using circuit-level modelling

M. Razm-Pa, F. Emami

Abstract. **We report a new circuit model for a self-assembled quantum-dot (SAQD) laser made of InGaAs/GaAs structures. The model is based on the excited state and standard rate equations, improves the previously suggested circuit models and also provides and investigates the performance of this kind of laser. The carrier dynamic effects on static and dynamic characteristics of a SAQD laser are analysed. The phonon bottleneck problem is simulated. Quantum-dot lasers are shown to be quite sensitive to the crystal quality outside and inside quantum dots. The effects of QD coverage factor, inhomogeneous broadening, the physical source of which is the size fluctuation of quantum dots formed by self-assembly of atoms, and cavity length on the SAQD laser characteristics are analysed. The results of simulation show that an increase in the cavity length and in the QD coverage factor results in the growth of the output power. On the other hand, an increase in the coverage factor and a degradation of inhomogeneous broadening lead to an increase in the modulation bandwidth. The effect of the QD height (cylindrical shape) and stripe width of the laser cavity on QD laser modulation is also analysed.**

Keywords: *self-assembled quantum-dot laser (SAQDL), inhomogeneous broadening, phonon bottleneck, coverage factor.*

1. Introduction

In many aspects including threshold current, modulation bandwidth and spectral bandwidth, semiconductor quantum-dot (QD) lasers show a much higher performance than conventional quantum-well (QW) lasers [1, 2]. In addition, QD lasers exhibit better carrier confinement compared to QW lasers due to three-dimensional confinement which makes them ideal candidates for special applications such as quantum information. The effect of real parameters of quantum dots, such as inhomogeneous broadening, phonon bottleneck, coverage factor and recombination time, on the dynamic and static characteristics of self-assembled QD lasers (SAQDLs) was studied in [3–6].

For better understanding of physics of QD lasers and their performance, we should take into account all the real parameters of QDs. Carrier relaxation rate in a quantum-dot discrete state plays a significant role in the entire performance of a QD laser. It has been shown that the carrier relaxation lifetime should be a few picoseconds less than a critical value in order to avoid the effect of the phonon bottleneck on the frequency behaviour [7]. The relaxation lifetime should be about 10 ps for high-power operation and about 1 ps for high-speed modulation (higher than 10 GHz). Meanwhile, the crystal quality outside and inside QDs also plays a significant role. To enhance the output power, an increase in the coverage factor and a decrease in inhomogeneous broadening are required.

The most useful and well-known method for studying the statics and dynamics of carriers and photons in these lasers involves the solution of rate equations [8]. Recently, some circuit models have been introduced for SAQDs, QW and bulk lasers [9]. However, in the previously suggested models, the excited state inside the active region energy band diagram is not considered. In this study, we take into account the excited state and then study the performance of QD lasers by improving previous rate equations and circuit models.

2. Theoretical background

Self-assembly in the fabrication of QD lasers allows one to have a wide variety of different semiconductor lasers. Depending on the discrete energy levels of a QD laser, one important aspect of SAQD lasers is the carrier relaxation (phonon bottleneck problem). Apart from this problem, in the case of single dots, the SAQDs characteristics are greatly affected by the inhomogeneous broadening of the optical gain, which, in fact, takes place due to the nonuniform sizes of quantum dots. Figure 1 shows the energy band diagram of a SAQD laser [10, 11].

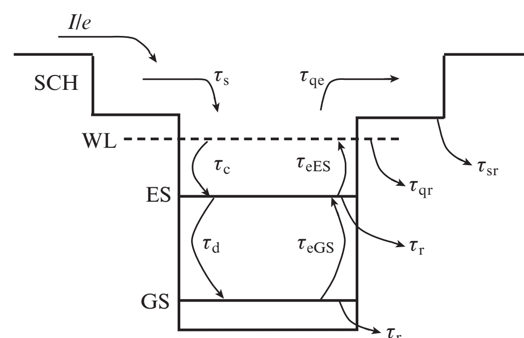

Figure 1. Energy band diagram of a SADQ laser with account for the excited state (see notations in the text).

M. Razm-Pa Electronic Department of Islamic Azad University, Boushehr, Iran; e-mail: Razmpa.mahdi@gmail.com;
F. Emami Optoelectronic Research Centre, Electronic Department of Shiraz University of Technology, Shiraz, Iran;
e-mail: emami@sutech.ac.ir

Received 17 June 2013
Kvantovaya Elektronika **45** (1) 15–22 (2015)
Submitted in English

In this model, there are some carriers injected into a separate confinement heterostructure (SCH) barrier with a rate I/e, where I is the injected current and e is the electron charge. The carriers can either relax with a rate τ_s^{-1} into the wetting layer (WL) state or come back from the barrier with a rate τ_{qe}^{-1}. These carriers can be captured by QDs of different sizes from the WL state. Assume that each dot has only two distinct energy states: ground state (GS) and excited state (ES). At these levels, the captured carriers have the relaxation rate τ_c^{-1} from the WL to the ES and the rate τ_d^{-1} from the ES to the GS. They can come back along the reverse path at the rates τ_{eES}^{-1} and τ_{eGS}^{-1}, respectively. There are several radiative or nonradiative recombination rates for carriers from the SCH with τ_{sr}^{-1}, from the WL with τ_{qr}^{-1} and from various bound states with τ_r^{-1}. Suppose that excited emission is only due to electron–hole recombination in the ES and the GS. The photons emitted from the laser cavity have a rate S/τ_p, where S is the number of photons and τ_p is the photon lifetime. Let us define the following parameters: the number of carriers in the SCH layer, N_s; in the WL layer, N_q; in the ES layer, N_{ES}; and in the GS layer, N_{GS}.

The governing rate equations for various components of these carriers have the form [5, 10–13]:

$$\frac{dN_s}{dt} = \frac{I}{e} - \frac{N_s}{\tau_s} - \frac{N_s}{\tau_{sr}} + \frac{N_q}{\tau_{qe}}, \tag{1a}$$

$$\frac{dN_q}{dt} = \frac{N_s}{\tau_s} + \frac{N_{ES}}{\tau_{eES}} - \frac{N_q}{\tau_{qr}} - \frac{N_q}{\tau_{qe}} - \frac{N_q}{\tau_c}, \tag{1b}$$

$$\frac{dN_{ES}}{dt} = \frac{N_q}{\tau_c} + \frac{N_{GS}(1-P_{ES})}{\tau_{eGS}} - \frac{N_{ES}}{\tau_r} - \frac{N_{ES}}{\tau_{eES}} - \frac{N_{ES}}{\tau_d} - \frac{(c/n_r) g^{(1)}_{mES} \Gamma}{1+\varepsilon_{mES}\Gamma S/V_a} S, \tag{1c}$$

$$\frac{dN_{GS}}{dt} = \frac{N_{ES}}{\tau_d} - \frac{N_{GS}}{\tau_r} - \frac{N_{GS}(1-P_{ES})}{\tau_{eGS}} - \frac{(c/n_r) g^{(1)}_{mGS} \Gamma}{1+\varepsilon_{mGS}\Gamma S/V_a} S, \tag{1d}$$

$$\frac{dS}{dt} = \frac{(c/n_r) g^{(1)}_{mES} \Gamma}{1+\varepsilon_{mES}\Gamma S/V_a} S + \frac{(c/n_r) g^{(1)}_{mGS} \Gamma}{1+\varepsilon_{mGS}\Gamma S/V_a} S - - \frac{S}{\tau_p} + \frac{\beta N_{GS}}{\tau_r} + \frac{\beta N_{ES}}{\tau_r}. \tag{1e}$$

Based on the density matrix theory, the linear optical gain of the active region at the dot density N_D can be found as [3, 5, 13]:

$$g^{(1)}_{mGS} = \frac{2.35\sqrt{2\pi}\, e^2 \hbar}{c n_r \varepsilon_0 m_0^2} \frac{|P^{\sigma}_{cv}|^2}{E_{GS}} \frac{2P_{GS}-1}{\Gamma_0} N_D D_{GS}, \tag{2}$$

$$g^{(1)}_{mES} = \frac{2.35\sqrt{2\pi}\, e^2 \hbar}{c n_r \varepsilon_0 m_0^2} \frac{|P^{\sigma}_{cv}|^2}{E_{ES}} \frac{2P_{ES}-1}{\Gamma_0} N_D D_{ES}, \tag{3}$$

where from [2, 3, 13]:

$$\varepsilon_{mGS} = \frac{e^2}{2 n_r^2 \varepsilon_0 m_0^2} \frac{|P^{\sigma}_{cv}|^2}{E_{GS}} \frac{1}{\Gamma_{cv}\Gamma_{\parallel}}; \tag{4}$$

$$\varepsilon_{mES} = \frac{e^2}{2 n_r^2 \varepsilon_0 m_0^2} \frac{|P^{\sigma}_{cv}|^2}{E_{ES}} \frac{1}{\Gamma_{cv}\Gamma_{\parallel}}; \tag{5}$$

$\Gamma_{\parallel} \equiv \tau_p^{-1}$ is the longitudinal relaxation rate; and Γ_{cv} is the scattering or polarisation dephasing rate. In the above equations, Γ is the optical confinement factor; Γ_0 is the inhomogeneous broadening of the optical gain; c is the speed of light; and β is the spontaneous coupling in/out efficiency. The photon lifetime τ_p can be found from [14]:

$$\tau_p^{-1} = \frac{c}{n_r}\left\{\alpha_i + \frac{\ln\left[(R_1 R_2)^{-1}\right]}{2L}\right\}, \tag{6}$$

where R_1 and R_2 are the left- and right-facet reflectivities of the laser cavity of length L with the internal loss α_i, and n_r is the cavity refractive index. Parameters D_{GS} and D_{ES} in Eqns (2) and (3) specify the GS and ES degeneracy which are considered to be 2 and 4, respectively. The matrix element P^{σ}_{cv}, related to the overlap integral I^{σ}_{cv} between the envelop functions of an electron and hole, is defined as [3, 14]:

$$|P^{\sigma}_{cv}|^2 = |I^{\sigma}_{cv}|^2 M^2, \tag{7}$$

where

$$M^2 = \frac{m_0^2}{12 m_e^*} \frac{E_g(E_g+\Delta)}{E_g + 2\Delta/3} \tag{8}$$

is the first-order k–p interaction between conduction and valence bands, with a separation E_g between the energy levels; m_e^* is the effective mass for electrons; and Δ is the spin-orbit interaction energy for the QD material. Based on Pauli's exclusion principle, the occupation probabilities in the ES and GS states of a QD are defined as [5]:

$$P_{GS} = \frac{N_{GS}}{2 N_D V_a D_{GS}}, \tag{9}$$

$$P_{ES} = \frac{N_{ES}}{2 N_D V_a D_{ES}}, \tag{10}$$

where $V_a = LWd$ is the cavity volume of length L, width W and thickness d.

The effect of the nonuniform dot size can be included in the expressions for the capture and escape times as follows [10, 11, 15]:

$$\tau_c = \frac{\tau_{c0}}{1-P_{ES}}, \tag{11}$$

$$\tau_d = \frac{\tau_{d0}}{1-P_{GS}}. \tag{12}$$

Here, τ_{c0} and τ_{d0} are the capture times from the WL to the ES and from the ES to the GS, respectively, with the assumption of the empty final state. Without stimulated emission and at room temperature, the system must converge to a quasi-thermal equilibrium based on a Fermi distribution. To have this condition met, the carrier capture time and the carrier escape time should satisfy the relations [10–12]:

$$\tau_{eGS} = \tau_{d0} \frac{D_{GS}}{D_{ES}} \exp\left(\frac{E_{ES}-E_{GS}}{kT}\right), \tag{13}$$

$$\tau_{eES} = \tau_{c0} \frac{D_{ES} N_d}{\rho_{WL_{eff}}} \exp\left(\frac{E_{WL}-E_{ES}}{kT}\right), \tag{14}$$

where

$$\rho_{WL_{eff}} \equiv \frac{m_{eWL} kT}{\pi \hbar^2} \tag{15}$$

is the effective density of states per unit area of the WL and N_d is the QD density per unit area. We assume that all the carriers are injected into the WL layer or equivalently $\tau_{qe} = \tau_{sr} \to \infty$.

3. Circuit model implementation

To solve the rate equations for a SAQD laser with the excited state taken into account, we propose an equivalent electrical circuit: the aforementioned equations are reduced to some simple electrical circuit equations and then the resulting circuit is simulated by a circuit simulator such as HSPICE [9]. To do this, we define the carrier populations in the SCH, WL and QD (in the ES and GS):

$$N_s = N_{s0}\exp\left(\frac{qV}{n_s kT}\right), \tag{16a}$$

$$N_q = N_{q0}\exp\left(\frac{qV_q}{n_q kT}\right), \tag{16b}$$

$$N_{ES} = N_{ES0}\exp\left(\frac{qV_{ES}}{n_{ES} kT}\right), \tag{16c}$$

$$N_{GS} = N_{GS0}\exp\left(\frac{qV_{GS}}{n_{GS} kT}\right), \tag{16d}$$

where N_{s0}, N_{q0}, N_{ES0} and N_{GS0} are the previously defined parameters in equilibrium; n_s, n_q, n_{ES} and n_{GS} are the diode ideality factors (for example, this factor is equal to 2 for AlGaAs [16, 17]); and V, V_q, V_{ES} and V_{GS} are the voltages applied to the structure, WL layer, QD excited state and QD ground state, respectively. To ensure a better convergence in the model, we define the laser output power by using a new parameter, V_m, in the form [18]:

$$P_{out} = (V_m + \delta)^2, \tag{17}$$

where δ is a small parameter (typically, 10^{-60}). It was shown [18] that for a set of nonlinear coupled rate equations, this choice can increase the convergence speed of the solutions.

Substituting (16a) in (1a) and after some mathematical manipulations, we have:

$$I = \frac{qN_{s0}}{2\tau_s}\left[\exp\left(\frac{qV}{n_s kT}\right) - 1 + \frac{2\tau_s q}{n_s kT}\exp\left(\frac{qV}{n_s kT}\right)\frac{dV}{dt}\right] + \frac{qN_{s0}}{2\tau_s}\left[\exp\left(\frac{qV}{n_s kT}\right) - 1\right] + \frac{qN_{s0}}{\tau_s}. \tag{18}$$

Here,

$$I_{D1} = \frac{qN_{s0}}{2\tau_s}\left[\exp\left(\frac{qV}{n_s kT}\right) - 1\right], \tag{19}$$

$$I_{D2} = \frac{qN_{s0}}{2\tau_s}\left[\exp\left(\frac{qV}{n_s kT}\right) - 1 + \frac{2\tau_s q}{n_s kT}\exp\left(\frac{qV}{n_s kT}\right)\frac{dV}{dt}\right], \tag{20}$$

$$I_{C1} = I_{C2} = \frac{qN_{s0}}{2\tau_s}, \tag{21}$$

$$I = I_{D1} + I_{C1} + I_{D2} + I_{C2}. \tag{22}$$

Substituting (16b) in (1b) and after some simplifications, we obtain

$$4I_{T1} + 2q\chi_1 N_{ES0}\exp\left(\frac{qV_{ES}}{n_{ES} kT}\right) = \frac{qN_{q0}}{\tau_{qr}}\left[\exp\left(\frac{qV_q}{n_q kT}\right) - 1 + \frac{2\tau_{qr} q}{n_q kT}\exp\left(\frac{qV_q}{n_q kT}\right)\frac{dV_q}{dt}\right] + \frac{qN_{q0}}{\tau_{qr}}\left[\exp\left(\frac{qV_q}{n_q kT}\right) - 1\right] + 2\frac{qN_{q0}}{\tau_{qr}} + 2q\zeta_1 N_{q0}\exp\left(\frac{qV_q}{n_q kT}\right), \tag{23}$$

$$I_{D3} = \frac{qN_{q0}}{\tau_{qr}}\left[\exp\left(\frac{qV_q}{n_q kT}\right) - 1\right], \tag{24}$$

$$I_{D4} = \frac{qN_{q0}}{\tau_{qr}}\left[\exp\left(\frac{qV_q}{n_q kT}\right) - 1 + \frac{2\tau_{qr} q}{n_q kT}\exp\left(\frac{qV_q}{n_q kT}\right)\frac{dV_q}{dt}\right], \tag{25}$$

$$I_{C3} = I_{C4} = \frac{qN_{q0}}{\tau_{qr}}, \tag{26}$$

$$G_1 = 2q\chi_1\Theta_2 I_{T6}, \tag{27}$$

$$G_2 = 2q\zeta_1\Theta_1 I_{T3}, \tag{28}$$

$$\chi_1 = \left(\frac{\rho_{WL_{eff}}}{D_{ES} N_d}\right)\tau_{c0}^{-1}\exp\left(-\frac{E_{WL} - E_{ES}}{kT}\right), \tag{29}$$

$$\zeta_1 = \frac{2N_D V_a D_{ES} - N_{ES}}{2N_D V_a D_{ES}\tau_{c0}}, \tag{30}$$

$$4I_{T1} + G_1 = I_{D4} + I_{D3} + I_{C4} + I_{C3} + G_2. \tag{31}$$

Substituting (16c) in (1c) and after some mathematical manipulations, we have

$$\frac{qN_{ES0}}{2\tau_r}\left[\exp\left(\frac{qV_{ES}}{n_{ES} kT}\right) - 1 + \frac{2\tau_r q}{n_{ES} kT}\exp\left(\frac{qV_{ES}}{n_{ES} kT}\right)\frac{dV_{ES}}{dt}\right] + \frac{qN_{ES0}}{\tau_r} + \frac{qN_{ES0}}{2\tau_r}\left[\exp\left(\frac{qV_{ES}}{n_{ES} kT}\right) - 1\right] + q\chi_1 N_{ES0}\exp\left(\frac{qV_{ES}}{n_{ES} kT}\right) + q\zeta_1 N_{ES0}\exp\left(\frac{qV_{ES}}{n_{ES} kT}\right) + \frac{q\alpha_{ES}}{\phi_{ES}[(V_m+\delta)^2]}(V_m+\delta)^2 = q\zeta_1 N_{q0}\exp\left(\frac{qV_q}{n_q kT}\right) + q\chi_2 N_{GS0}\exp\left(\frac{qV_{GS}}{n_{GS} kT}\right), \tag{32}$$

$$I_{D5} = \frac{qN_{ES0}}{2\tau_r}\left[\exp\left(\frac{qV_{ES}}{n_{ES} kT}\right) - 1 + \frac{2\tau_r q}{n_{ES} kT}\exp\left(\frac{qV_{ES}}{n_{ES} kT}\right)\frac{dV_{ES}}{dt}\right], \tag{33}$$

$$I_{D6} = \frac{qN_{ES0}}{2\tau_r}\left[\exp\left(\frac{qV_{ES}}{n_{ES} kT}\right) - 1\right], \tag{34}$$

$$I_{C3} = I_{C6} = \frac{qN_{ES0}}{2\tau_r}, \tag{35}$$

$$G_3 = q\zeta_1\Theta_1 I_{T3}, \tag{36}$$

$$G_4 = q\chi_2\Theta_2 I_{T8}, \tag{37}$$

$$G_5 = q\chi_1\Theta_2 I_{T6}, \tag{38}$$

$$G_6 = q\zeta_2\Theta_2 I_{T6}, \tag{39}$$

$$G_7 = \frac{q\alpha_{ES}}{\phi_{ES}[(V_m+\delta)^2]}(V_m+\delta)^2, \tag{40}$$

$$\chi_2 = \frac{2N_D V_a D_{ES} - N_{ES}}{2N_D V_a D_{ES}}\tau_{eES}^{-1}, \tag{41}$$

$$\zeta_2 = \frac{2N_D V_a D_{GS} - N_{GS}}{2N_D V_a D_{GS}}\tau_{d0}^{-1}, \tag{42}$$

$$G_3 + G_4 = I_{D5} + I_{D6} + I_{C5} + I_{C6} + G_5 + G_6 + G_7. \tag{43}$$

And finally, after substituting (16d) in (1d), we will have

$$\frac{qN_{GS0}}{2\tau_r}\left[\exp\left(\frac{qV_{GS}}{n_{GS}kT}\right) - 1 + \frac{2\tau_r q}{n_{GS}kT}\exp\left(\frac{qV_{GS}}{n_{GS}kT}\right)\frac{dV_{GS}}{dt}\right]$$
$$+\frac{qN_{GS0}}{\tau_r} + \frac{qN_{GS0}}{2\tau_r}\left[\exp\left(\frac{qV_{GS}}{n_{GS}kT}\right) - 1\right] + q\chi_2 N_{GS0}\exp\left(\frac{qV_{GS}}{n_{GS}kT}\right)$$
$$+\frac{q\alpha_{GS}}{\phi_{GS}[(V_m+\delta)^2]}(V_m+\delta)^2 = q\zeta_2 N_{ES0}\exp\left(\frac{qV_{ES}}{n_{ES}kT}\right), \tag{44}$$

$$I_{D7} = \frac{qN_{GS0}}{2\tau_r}\left[\exp\left(\frac{qV_{GS}}{n_{GS}kT}\right) - 1 + \frac{2\tau_r q}{n_{GS}kT}\exp\left(\frac{qV_{GS}}{n_{GS}kT}\right)\frac{dV_{GS}}{dt}\right], \tag{45}$$

$$I_{D8} = \frac{qN_{GS0}}{2\tau_r}\left[\exp\left(\frac{qV_{GS}}{n_{GS}kT}\right) - 1\right], \tag{46}$$

$$I_{C7} = I_{C8} = \frac{qN_{GS0}}{2\tau_r}, \tag{47}$$

$$G_8 = q\zeta_2\Theta_2 I_{T6}, \tag{48}$$

$$G_9 = q\chi_2\Theta_2 I_{T3}, \tag{49}$$

$$G_{10} = \frac{q\alpha_{GS}}{\phi_{GS}[(V_m+\delta)^2]}(V_m+\delta)^2, \tag{50}$$

$$G_8 = I_{D7} + I_{D8} + I_{C7} + I_{C8} + G_9 + G_{10}. \tag{51}$$

Also, we have

$$2\tau_p\frac{dV_m}{dt} + V_m = \frac{\tau_p\alpha_{ES}}{\phi_{ES}(S)}(V_m+\delta) - \frac{\delta}{2}$$
$$+\frac{\tau_p\alpha_{GS}}{\phi_{GS}(S)}(V_m+\delta) - \frac{\delta}{2} + \frac{\tau_p\beta N_{ES}}{\tau_r(V_m+\delta)} + \frac{\tau_p\beta N_{GS}}{\tau_r(V_m+\delta)}, \tag{52}$$

$$C_{ph} = 2\tau_p, \quad R_{ph} = 1, \tag{53}$$

$$G_{11} = \frac{\tau_p\beta N_{ES}}{\vartheta\tau_r(V_m+\delta)}, \tag{54}$$

$$G_{12} = \frac{\tau_p\beta N_{GS}}{\tau_r(V_m+\delta)}, \tag{55}$$

$$G_{13} = \frac{\tau_p\alpha_{GS}}{\phi_{GS}(S)}(V_m+\delta) - \frac{\delta}{2}, \tag{56}$$

$$G_{14} = \frac{\tau_p\alpha_{GS}}{\phi_{GS}(S)}(V_m+\delta) - \frac{\delta}{2}, \tag{57}$$

$$C_{ph}\frac{dV_m}{dt} + \frac{V_m}{R_{ph}} = G_{11} + G_{12} + G_{13} + G_{14}, \tag{58}$$

$$\vartheta = \frac{S}{P_{out}} = \frac{\lambda\tau_p}{\eta_c V_a hc}, \tag{59}$$

$$\alpha_{GS} = \frac{2.35\sqrt{2\pi}e^2\hbar}{cn_r\varepsilon_0 m_0^2}\frac{|P_{cv}^{\sigma}|^2}{E_{GS}}\frac{1}{\Gamma_0}\left(\frac{N_{GS}}{N_D V_a D_{GS}} - 1\right)\frac{c}{n_r}\Gamma N_D D_{GS}, \tag{60}$$

$$\alpha_{ES} = \frac{2.35\sqrt{2\pi}e^2\hbar}{cn_r\varepsilon_0 m_0^2}\frac{|P_{cv}^{\sigma}|^2}{E_{ES}}\frac{1}{\Gamma_0}\left(\frac{N_{ES}}{N_D V_a D_{ES}} - 1\right)\frac{c}{n_r}\Gamma N_D D_{ES}, \tag{61}$$

$$\phi_{ES}(S) = 1 + \frac{\varepsilon_{mES}\Gamma S}{V_a}, \tag{62}$$

$$\phi_{GS}(S) = 1 + \frac{\varepsilon_{mGS}\Gamma S}{V_a}, \tag{63}$$

$$\Theta_1 = \frac{\tau_{qr}}{q},\ \Theta_2 = \frac{2\tau_r}{q},\ N_q = \Theta_1 I_{T3}, N_{ES} = \Theta_2 I_{T6},\ N_{GS} = \Theta_2 I_{T8}, \tag{64}$$

Here, η_c is the coupling coefficient for the output power.

In these relations E_{out} is related to V_m in the output power P_{out} by the equation:

$$P_{out} = E_{out} = (V_m + \delta)^2. \tag{65}$$

Taking into account the above equations, it is possible to obtain an equivalent circuit shown in Fig. 2. In this circuit, p and n are the electrical terminals for a SAQD laser, and P_{out} is a terminal the output voltage at which can determine the output laser power. For SCH carriers, charge storage and carrier capturing are done by current sources D_1, D_2 and I_{C1}, I_{C2}, respectively. Also, current sources D_3 and D_4 can be used to model the charge storage in the WL, and current sources I_{C3} and I_{C4} represent the emission from this layer, whereas G_2 explains the carrier recombination effects. The current source $4I_{T1}$ and G_1 are used for explaining the capturing effects in the WL. For charge storage and carrier emission from QDs (in the ES and GS), this model uses the current sources D_5, D_6 together with I_{C5}, I_{C6} and D_7, D_8 together with I_{C7}, I_{C8}. Conductances G_3, G_6 and G_5 explain the effect of carrier recombination and carrier capturing in the WL, and G_4 and G_7 represent the carrier capturing and stimulated emission effects in the GS of this SAQD laser. In a similar manner, G_8, G_9 and G_{10} represent the carrier capturing and stimulated emission effects in the ES. By varying the photon density in time with spontaneous and stimulated emissions taken into account, we have modelled R_{ph} and C_{ph}, which are specified by G_{11}, G_{12} and G_{13}, G_{14}. Finally, E_{out} is equal to the output laser power at a fixed voltage [see Eqn (64)]. In this simulation we used typical parameters [3, 9–11]. The parameters of the QD material are as follows: τ_s = 6 ns, τ_{sr} = 4.5 ns, τ_{qr} = 3 ns, τ_{c0} = 1 ps, τ_{d0} = 7 ps, τ_r = 2.8 ns, E_{GS} = 0.96 eV, E_{ES} = 1.04 eV, Δ = 0.35 eV, Γ_0 = 20 meV, distance between energy levels of the SCH and WL states is 84 meV, and average distance between the energy levels of the WL and ES states is 100 meV and the ES and GS states is 80 meV. The parameters of the laser are as follows: active region length, L_{ca} = 900 μm; SCH layer thickness, H_b = 90 nm; WL layer thickness, H_{WL} = 1 nm; W = 10 μm; $V_a = 2.2 \times 10^{-16}$ m^3; $N_d = 5 \times 10^{10}$ cm^{-2}; $N_D = 6.3 \times 10^{22}$ m^{-3}; Γ = 0.06; α_i = 1 cm^{-1}; $\beta = 10^{-4}$; η_c = 0.449; $n_s = n_q = n_{GS} = n_{ES} = 2$, R_1 = 30%; and R_2 = 90%.

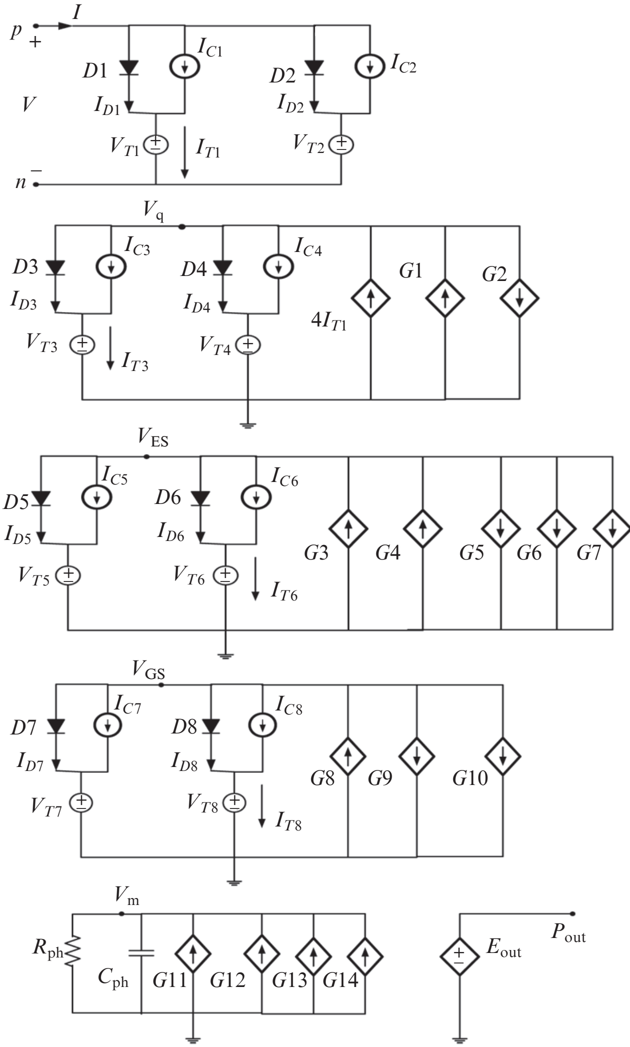

Figure 2. Circuit simulation of the rate equations for a SAQD laser with the excited state taken into account.

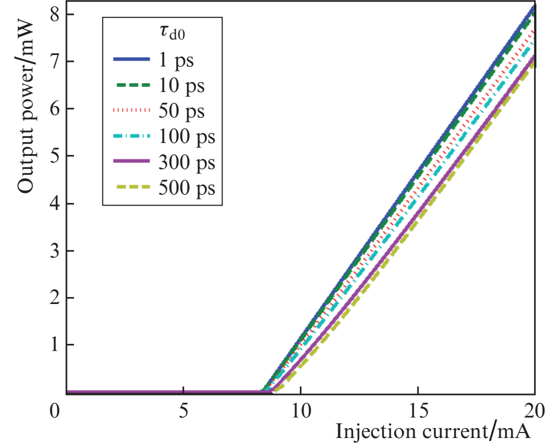

Figure 3. $L-I$ curve of a SAQD laser at different τ_{d0}; $\tau_r = 2.8$ ns, $\tau_{qr} = 0.5$ ns and $\tau_{c0} = 10$ ps.

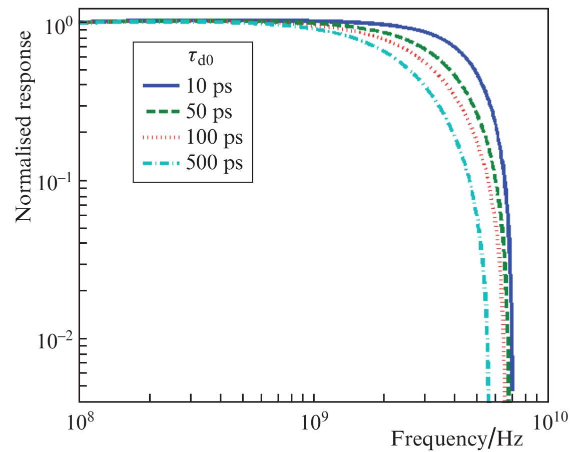

Figure 4. Frequency response of a SAQD laser at different τ_{d0}; $\tau_r = 2.8$ ns, $\tau_{qr} = 3$ ns, $\tau_{c0} = 10$ ps.

4. Simulation results

By using the proposed model and a circuit simulator such as HSPICE, the SAQD laser behaviour is studied. Results are plotted in Fig. 3. One can see that longer lifetimes correspond to larger threshold currents. This is accompanied by lowering the slopes of the output power curves, which means lower quantum efficiencies for increased lifetimes. Physically, this effect is due to the phonon bottleneck in QD lasers. Unlike [9], in this work we consider the excited states in QDs and hence the effects of the carrier escape from ground state to the excited state and from the excited state to the wetting layer, which are neglected in Ref. [9]. On the other hand, due to the carrier escaping mechanism, the number of carriers in the WL increases and these carriers are consumed in the form of non-radiative recombination so that the threshold current will be increased. Thus, at higher relaxation times τ_{d0}, the frequency response deteriorates and the SAQD laser can have lower bandwidths (Fig. 4).

Figure 5 shows the results of our simulations on the $L-I$ curve of a SAQD laser with account for the inhomogeneous broadening effects, which is explained by a scatter in the QD sizes [3]. One can see from Fig. 5 that although at a higher inhomogeneous broadening factor Γ_0, greater threshold currents (or equivalently higher injection currents) are needed, the external quantum efficiency does not exhibit any dominant changes. In other words, at higher Γ_0 the output laser

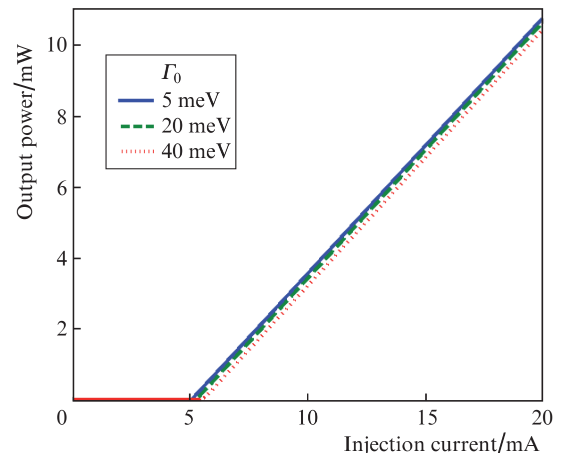

Figure 5. $L-I$ curve of a SAQD laser with the excited state taken into account at different Γ_0; $\tau_r = 2.8$ ns, $\tau_{qr} = 3$ ns, $\tau_{c0} = 10$ ns, $\tau_{d0} = 7$ ps.

power decreases. Indeed, when the inhomogeneous broadening factor Γ_0 increases, higher occupation probabilities take place in the lasinge, so that the relaxation times increase and the output power decreases. This effect can be studied in the dynamic response of a SAQD laser (Fig. 6). The results of simulations show that at higher inhomogeneous broadening factors the frequency responses of the laser deteriorates.

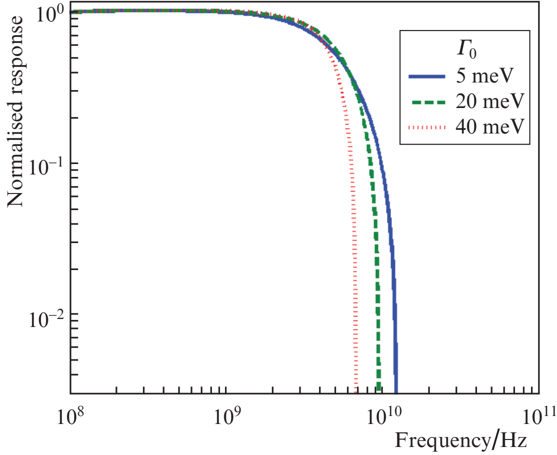

Figure 6. Frequency response of a SAQD laser at different Γ_0; $\tau_r = \tau_{qr} =$ 2.8 ns.

The effect of carrier recombination time τ_{qr} in a QW, which depends on the QW crystal quality, is shown by the $L-I$ curve in Fig. 7. As τ_{qr} decreases, the carriers find more opportunities to recombine through nonradiatve processes outside of the QT, which results in degradation of the external quantum efficiency. One can see from Fig. 7 that τ_{qr} degradation also increases the threshold current. The effect of the carrier recombination in the WL state on the small-signal frequency response of the laser is shown in Fig. 8. One can see that the carrier recombination in the WL state has no considerable effect on the modulation response. Figure 9 shows the effect of carrier recombination time τ_r inside the QD on the $L-I$ curve. While the effect of τ_r on threshold current is significant, it does not have any considerable effect on the external quantum efficiency. The effect of τ_r on the frequency characteristic is shown in Fig. 10. It is important to note that as τ_r decreases from 2.8 to 0.5 ns, the frequency response deteriorates. Therefore, to prevent the effect of the phonon bottleneck on the frequency response, the recombination lifetime inside the QD, τ_r, must be much longer than the carrier relaxation time (the carrier relaxation time is about a few picoseconds).

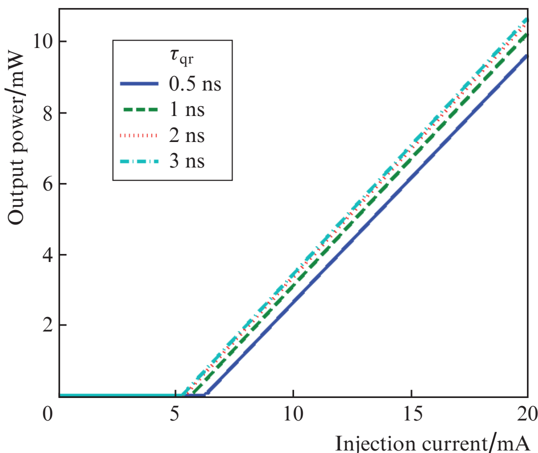

Figure 7. $L-I$ curve of a SAQD laser at different τ_{qr}; $\tau_r = 2.8$ ns, $\tau_{c0} =$ 10 ns, $\tau_{d0} = 7$ ps.

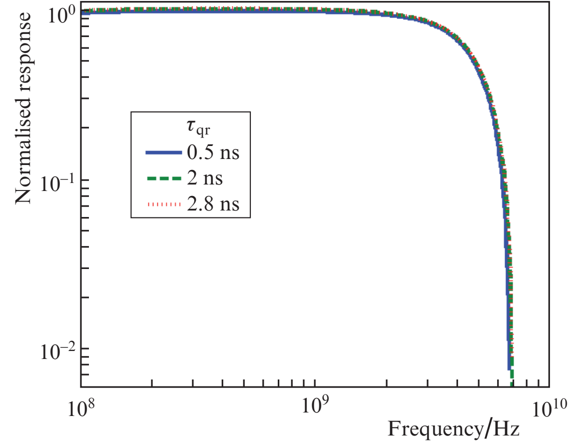

Figure 8. Modulation response of a SAQD laser at different τ_{qr}; $\tau_r =$ 2.8 ns, $\tau_{c0} = 10$ ns, $\tau_{d0} = 7$ ps.

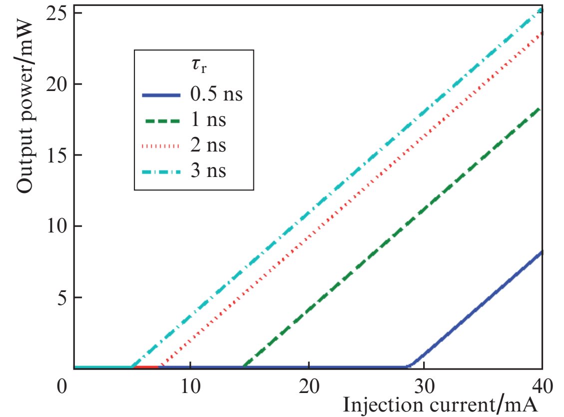

Figure 9. $L-I$ curve of a SAQD laser at different τ_r.

The effect of the carrier escape time from the GS to the ES and from the ES to the WL state on the $L-I$ curve is shown in Fig. 11. As the carrier escape time decreases, the number of carriers in the WL state (N_q) increases. These carriers participate in the nonradiative recombination (with τ_{qr} lifetime), which leads to an increase in the threshold current. Generally, the lower the τ_{qr} value, the higher the threshold current. Figure 12 also shows that as the carrier escape time from the GS to the ES and from the ES to the WL decreases, the frequency response degrades as well.

Figure 13 show the frequency response at different QD coverage factors ξ. One can see that an increase in ξ with increasing volumetric density of QDs (N_D) leads to a decrease in filling probabilities P_{GS} and P_{ES} of the GS and ES. In this case, the relaxation rate of the carriers inside the GS and ES increases, which finally leads to an increase in the bandwidth at a 3-dB level. Figure 14 shows the frequency response at dif-

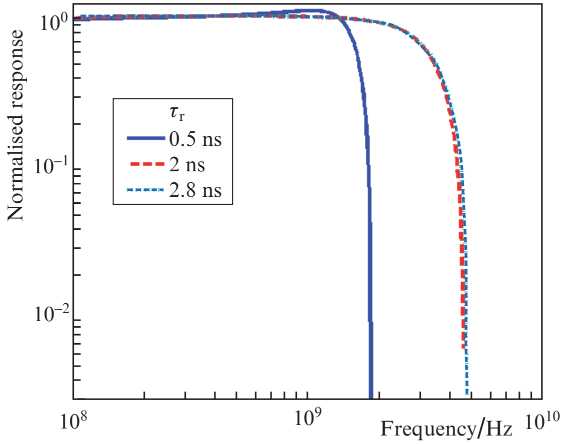

Figure 10. Modulation response of a SAQD laser at different τ_r.

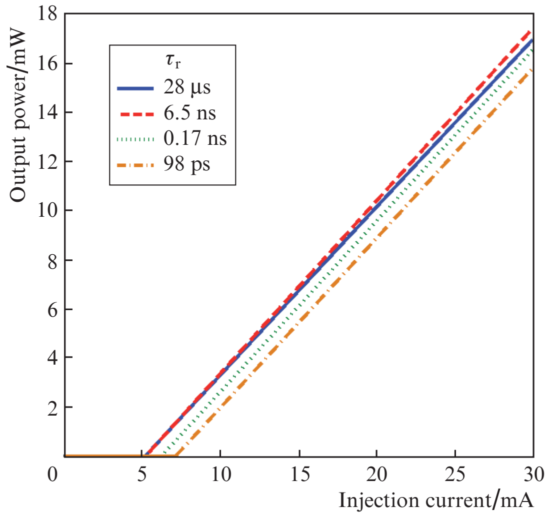

Figure 11. $L-I$ curve of a SAQD laser at different carrier escape times from the GS to the ES and from the ES to the WL.

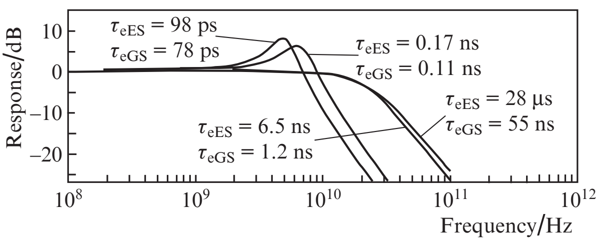

Figure 12. Modulation response of a SAQD laser at different carrier escape times from the GS to the ES and from the ES to the WL.

ferent overage factors, Γ_0 = 5 meV and relaxation time equal to 1 ps. To achieve a high-speed (higher than 10 GHz) modulation, one should decrease the relaxation lifetime down to about 1 ps, to increase the QD coverage factor and to decrease the inhomogeneous broadening.

Figure 15 shows the $L-I$ characteristics of the laser at different cavity lengths L. An increase in L is accompanied by a decrease in losses and an increase in the output power. Figure 16 shows the modulation response at different QD heights. One can see that as the QD height decreases, the

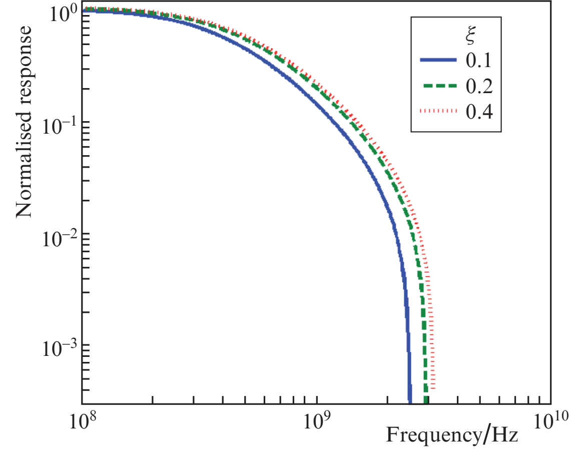

Figure 13. Modulation response of a SAQD laser at different coverage factors; Γ_0 = 20 meV and the relaxation time is 100 ps.

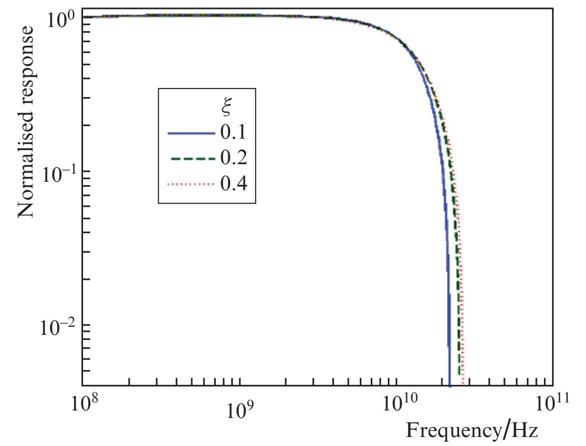

Figure 14. Modulation response of a SAQD laser at different coverage factors; Γ_0 = 5 meV and the relaxation time is 1 ps.

modulation bandwidth improves. The reason for the modulation bandwidth improvement consists in an increase in the

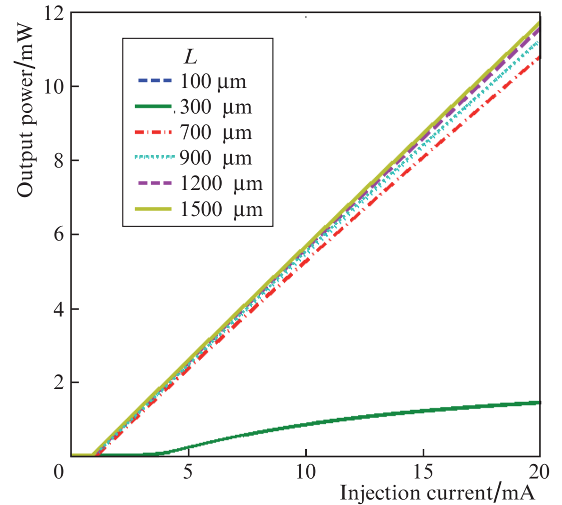

Figure 15. $L-I$ curve of a SAQD laser at different cavity lengths.

carrier confinement inside QDs in growth direction (along the *z* axis), which in turn leads to an increase in the excited stimulated emission rate. Figure 17 shows the effect of the stripe width of the laser cavity on the frequency response. As the stripe width of the laser cavity decreases, the modulation bandwidth improves. Indeed, a decrease in the stripe width of the laser cavity and therefore a degradation of the active region can provide a higher total capture rate. Hence, it results in a greater modulation bandwidth.

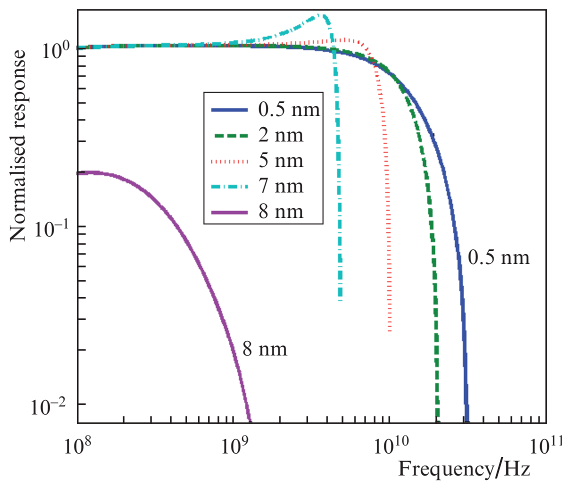

Figure 16. Modulation response of a SAQD laser at different QD heights.

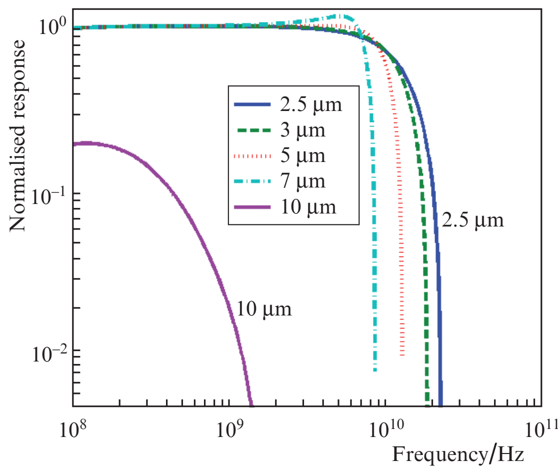

Figure 17. Modulation response of a SAQD laser at different stripe widths of the laser cavity.

5. Conclusions

Using the proposed equivalent circuit model we have simulated an InGaAs/GaAs SAQD laser with allowance of the ES role in the active region. In these simulations, important laser parameters, such as the L–I curve and the modulation response are calculated by using a circuit simulator. It is found that, at longer capture times the threshold current increases whereas the output power, laser bandwidths and the quantum efficiency decrease. It is shown that an increase in the QD coverage factor and the cavity length and a decrease in the inhomogeneous broadening lead to an increase in the output power. In addition, an increase in the QD coverage factor and a decrease in the inhomogeneous broadening and in the relaxation time can result in a growth of the frequency bandwidth. It is also shown that a decrease in the recombination time of the WL state causes a degradation of the external quantum efficiency and a growth of the threshold current while this recombination time does not have any significant effect on the modulation response. On the other hand, a decrease in the recombination time inside the QD not only increases the threshold current but also degrades the modulation bandwidth. A decrease in the carrier escape time from the GS to the ES and from the ES to the WL state increases the threshold current and deteriorates the frequency response. We have suggested that a decrease in the QD height and stripe width of the laser cavity improves the modulation bandwidth.

References

1. Fiore A., Markus A. *IEEE J. Quantum Electron.*, **43** (4), 287 (2007).
2. Grundmann M. *Nano-Optoelectronics, Concepts, Physics and Devices* (New York: Springer, 2002).
3. Sugawara M., in: *Semiconductors and Semimetals* (San Diego, CA: Academic, 1999) Vol. 60.
4. Sugawara M., Mukai K., Shoj H. *Appl. Phys. Lett.*, **71** (19), 2791 (1997).
5. Sugawara M., Hatori N., Ebe H., Ishida M. *J. Appl. Phys.*, **97** (4), 43523 (2005).
6. Ohnesorge B., Albrecht M., Oshinowo J., Forchel A., Arakawa Y. *Phys. Rev. B*, **54** (16), 11532 (1996).
7. Ahmadi V., Yavari M.H. *IEEE J. Sel. Top. Quantum Electron.*, **17** (5), 1153 (2011).
8. Sugawara M., Mukai K., Nakata Y., Ishikawa H., Sakamoto A. *Phys. Rev. B*, **61** (11), 7595 (2000).
9. Ahmadi V., Yavari M.H. *IEEE J. Sel. Top. Quantum Electron.*, **15** (3), 774 (2009).
10. Gioannini M., Sevega A., Montrosset I. *Opt. Quantum Electron.*, **38**, 381 (2006).
11. Gioannini M., Montrosset I. *IEEE J. Quantum Electron.*, **43**, 941 (2007).
12. Markus A., Chen J.X., Gauthier-Lafaye O., Provost J.G., Paranthoën C., Fiore A. *IEEE J. Sel. Top. Quantum Electron.*, **9** (5), 1308 (2003).
13. Grillot F., Veselinov K., Gioannini M., Montrosset I., Even J., Piron R., Homeyer E., Loualiche S. *IEEE J. Quantum Electron.*, **45** (7), 872 (2009).
14. Sugawara M. *Proc. SPIE Int. Soc. Opt. Eng.*, **3283**, 88 (1998).
15. Berg T., Bischoff S., Magnusdottir I., Mork J.R. *IEEE Photonics Technol. Lett.*, **13** (6), 541 (2001).
16. Tucker R.S., Pope D.J. *IEEE J. Quantum Electron.*, **QE-19** (7), 1179 (1983).
17. Katz J., Margalit S., Harder C., Wilt D., Yariv A. *IEEE J. Quantum Electron.*, **QE-17** (1), 4 (1981).
18. Mena P.V., Kang S.M., DeTemple T.A. *J. Lightwave Technol.*, **15** (4), 717 (1997).